Available online at www.sciencedirect.com
ScienceDirect
Progress in Nuclear Energy 50 (2008) 730–739
PROGRESS IN NUCLEAR ENERGY
An International Review Journal
www.elsevier.com/locate/pnucene

The IRIS pressurizer: Simulation of out-surge transients and optimization procedure to design scaled experiments

David A. Botelho [a], Paulo A.B. De Sampaio [a], Celso M.F. Lapa [a], Cláudio M.N.A. Pereira [a], Maria de Lourdes Moreira [a,*], Antônio Carlos de O. Barroso [b]

[a] *Instituto de Engenharia Nuclear, Rio de Janeiro, Brazil*
[b] *Instituto de Pesquisas Energéticas e Nucleares, São Paulo, Brazil*

Abstract

Numeric models of the IRIS reactor pressurizer having either two or three volumes were employed to simulate a typical out-surge transient. The vapor volume may contain liquid drops. Vapor bubbles can be generated in the liquid volume. The mass, the energy, the constitutive, and the state equations, represent all relevant phenomena. A pressure equation is derived by the substitution of the mass and energy equations onto the pressurizer volume constraint, assuming that the instantaneous pressure is the same in all volumes. The pressurizer experimental data of a loss of load transient in the Shippingport reactor are used to validate these pressurizer models. These models are also employed to verify the capacity of the thermal power controller to restore the pressure in the IRIS out-surge transient. The preliminary validation, using the Shippingport experimental data, and the close agreement reached by all the developed software, for the IRIS out-surge transient, recommends further validation of these models for the test evaluation and the design of scaled experiments for the IRIS pressurizer.

The proper choice of the pressure number was employed to obtain the best form of the non-dimensional conservation equations for a two-volume pressurizer. This form and the non-dimensional constitutive models, define the similarity numbers of scaled systems similar to the IRIS reactor pressurizer. The similarity numbers represent the scaled transport of mass and energy, and of the local rainout, flashing, and wall condensation mass and energy transport. The genetic algorithm (GA) search variables of scaled models are the geometric sizes, the surge mass flow rate, and the heater power needed to control the pressure. The similarity numbers are used to define a ''fitness function'' to evaluate the quality of the defined variables. The operation of the systems is verified using a two-volume transient model to simulate a typical out-surge transient. The agreement of the non-dimensional pressure as the model pressure increases, and the good agreement of the non-dimensional volumes of different scaled systems recommends this non-dimensional formalism, the GA optimization, and the numeric simulation of a surge transient, to design scaled experiments for modeling the IRIS pressurizer.

Keywords: Nuclear reactor; Pressurizer simulation; Scaled experiment; Optimization procedure

1. Introduction

The IRIS reactor, steam generator and primary pumps are contained within an integral vessel. The pressurizer is contained within the integral vessel upper head. It has a larger steam volume for the reactor core power than the current PWRs. Because of its large volume, the IRIS pressurizer does not need a spray system of sub-cooled liquid to reduce pressure increments due to in-surge transients, but heaters are provided in the lowest liquid volume. The lowest liquid volume of the pressurizer is separated from the circulating reactor coolant by a dividing steel structure that contains the surge flow path. Part of the pressurizer test scope is the simulation of surges in and out of the pressurizer, and the simulation of the heater operating modes.

2. Mass and energy conservation equations

The three-volume model consists of an upper volume of vapor, an intermediate volume of liquid situated in part of the hemispheric volume, and a fixed volume of liquid located

* Corresponding author.
E-mail address: malu@ien.gov.br (M. de. L. Moreira).

0149-1970/$ - see front matter © 2008 Elsevier Ltd. All rights reserved.
doi:10.1016/j.pnucene.2007.12.006

Nomenclature

A	flow area
Fr	Froude number
h	enthalpy per unit mass
k	thermal conductivity
K_p	proportional constant of the PI controller
K_i	integral constant of the PI controller
L	length
m	mass
$\dot{m}, W$	mass flow rate
$N_0 = NW_{WC}$	mass flow wall condensation number
$N_1 = NW_{RO}$	rainout number
$N_2 = N\dot{Q}_{WC}$	wall condensation heat number
$N_3 = NW_{FL}$	flashing number
$N_4 = \Psi$	pressure number
$N_5 = NK_i$	integral pressure control number
$N_6 = NK_p$	proportional pressure control number
$N_7 = (NWh_{RO})_1$	first enthalpy transport rainout number
$N_8 = (NWh_{RO})_2$	second enthalpy transport rainout number
$N_9 = (NWh_{FL})_1$	first enthalpy transport flashing number
$N_{10} = (NWh_{FL})_2$	second enthalpy transport flashing number
$N_{11} = (NWh_{WC})_1$	first enthalpy transport wall condensation number
$N_{12} = (NWh_{WC})_2$	second enthalpy transport wall condensation number
$N_{13} = (NWh_{WC})_3$	third enthalpy transport wall condensation number
$N_{14} = (NWh_{WC})_4$	fourth enthalpy transport wall condensation number
p	pressure
$\dot{Q}$	thermal power
S	wall area
T	temperature
t	time
u	velocity
V	volume
$v = x(v_g/\alpha) = ((h-h_f)/h_{fg})(v_g/\alpha)$	volume per unit mass
$x = (h-h_f)/h_{fg}$	steam quality
$\alpha = x(v_g/v)$	vapor (void) fraction
γ_l	bubble non-dimensional velocity
ρ	density
μ	viscosity
σ	surface tension

Subscripts

FL	flashing
RO	rainout
WC	wall condensation
0	reference value
PI	proportional-integral
p	proportional
i	integral
f	saturated liquid
g	saturated vapor
l	liquid volume
v	vapor volume

in a cylinder below the pressurizer hemisphere. In the two-volume model, the liquid volumes are collapsed in one volume that spreads from part of the liquid hemispheric volume to the liquid in the lower cylinder. The mass conservation equations are written in terms of the mass flow rates crossing internal interfaces and the surge interface. The internal energy conservation equations are written in terms of the convective heat rate, the thermal power, and the mechanical power (Todreas and Kazimi, 1990). The mechanical power is defined as the pressure times the volume rates. The mass conservation equations for the vapor, the upper liquid, and the lower liquid of the pressurizer are

$$\frac{d}{dt}(m_v) = W_{FL_1} - W_{RO} - W_{WC} - \dot{m}_{l_1 v} \tag{1}$$

$$\frac{d}{dt}(m_{l_1}) = W_{FL_2} - W_{FL_1} + W_{RO} + W_{WC} + \dot{m}_{l_1 l_2} + \dot{m}_{l_1 v} \tag{2}$$

$$\frac{d}{dt}(m_{l_2}) = \dot{m}_{surge} - W_{FL_2} - \dot{m}_{l_1 l_2} \tag{3}$$

The energy conservation equations for the vapor, the upper liquid, and the lower liquid of the pressurizer are

$$\frac{d}{dt}(m_v h_v) = (W_{FL_1} - W_{WC})h_g - W_{RO}h_f - \dot{Q}_{l_1 v} - \dot{Q}_{wv} - \dot{m}_{l_1 v}h_{l_1 v} + (m_v v_v)\frac{dp}{dt} \tag{4}$$

$$\frac{d}{dt}(m_{l_1}h_{l_1}) = (W_{RO} + W_{WC})h_f + (W_{FL_2} - W_{FL_1})h_g + (m_{l_1}v_{l_1})\frac{dp}{dt} + \dot{Q}_{l_1 v} + \dot{m}_{l_1 v}h_{l_1 v} - \dot{Q}_{l_1 l_2} - \dot{Q}_{wl_1} + \dot{m}_{l_1 l_2}h_{l_1 l_2} \tag{5}$$

$$\frac{d}{dt}(m_{l_2}h_{l_2}) = \dot{m}_{surge}h_{surge} - W_{FL_2}h_g + \dot{Q}_{l_1 l_2} - \dot{Q}_{wl_2} - \dot{m}_{l_1 l_2}h_{l_1 l_2} + \dot{Q}_{heater} + (m_{l_2}v_{l_2})\frac{dp}{dt} \tag{6}$$

In the three-volume model, the lower liquid volume is fixed. This constraint condition is used to calculate the mass flow rate on the interface between the two liquid volumes. The mass flow rate equation is derived by the substitution of the mass balance equation of the lower liquid volume into the volume constraint condition. The final result is (Barroso and Batista Fo, 2004; Barroso et al., 2003)

$$\dot{m}_{l_1 l_2}^{(t+\Delta t)} = \dot{m}_{\text{surge}}^{(t+\Delta t)} - W_{\text{FL}_2}^{(t+\Delta t)} + \frac{\left(m_{l_2}^{(t)}\right)^2}{\text{Vol}_{l_2}} \times \left[\left(\frac{\partial v_{l_2}}{\partial h_{l_2}}\right)_p \frac{h_{l_2}^{(t)} - h_{l_2}^{(t-\Delta t)}}{\Delta t} + \left(\frac{\partial v_{l_2}}{\partial p}\right)_{h_{l_2}} \frac{p^{(t)} - p^{(t-\Delta t)}}{\Delta t}\right] \tag{7}$$

The total volume of the pressurizer is also invariant with time. As the lower liquid volume is fixed, the remaining volume constraint condition is used to derive the following pressure equation

$$v_v \frac{dm_v}{dt} + v_{l_1} \frac{dm_{l_1}}{dt} + \left(\frac{\partial v_v}{\partial h_v}\right)_p m_v \frac{dh_v}{dt} + \left(\frac{\partial v_{l_1}}{\partial h_{l_1}}\right)_p m_{l_1} \frac{dh_{l_1}}{dt} + \left[m_{l_1}\left(\frac{\partial v_{l_1}}{\partial p}\right)_{h_{l_1}} + m_v \left(\frac{\partial v_v}{\partial p}\right)_{h_v}\right] \frac{dp}{dt} = 0 \tag{8}$$

The substitution of the vapor and the upper liquid volume mass balance equations and energy balance equations into Eq. (8) finalizes the derivation of the pressure differential equation. Closure constitutive relations define the unknown mass flow rates. Liquid and steam thermodynamic state equations are also used for closure.

3. Constitutive models

The heat diffusion from the lower liquid volume to the middle liquid volume is neglected. The mass exchange on the interface of the vapor volume and the middle liquid volume is calculated using the gas kinetic theory. The heat exchange on the interface of the vapor volume and the middle liquid volume is calculated using a convective heat transfer coefficient (Kang and Griffith, 1984).

Liquid drops are generated in the vapor volume due to bulk condensation (rainout) (Baron, 1973; Nahavandi and Makkenchery, 1970). Due to the large density of a liquid drop as compared to the density of the vapor volume, the drops never reach speeds needed for significant drag force. Thus the liquid drops reach the interface with the velocity of a free falling body. They enter the liquid volume through the liquid interface. The rainout mass flow rate is defined in terms of the interface area, the liquid fraction in the vapor volume, and the drop final velocity in the vapor volume.

Vapor bubbles are generated in the liquid volume due to bulk evaporation (flashing) (Baron, 1973; Nahavandi and Makkenchery, 1970). Due to the small density of the vapor bubble as compared to that of the liquid volume, the drops can have a significant (buoyancy minus gravity) acceleration. Thus they reach sufficient speed for significant drag force. The flashing mass flow rate is defined in terms of the interface area, the vapor fraction in the liquid volume, and bubble terminal velocity in the liquid volume, that is calculated using the Wilson formula (Wilson et al., 1961). The transient rainout and flashing mass flow rates are calculated employing a transit time delay model (Nahavandi and Makkenchery, 1970).

The mass flow rate due to vapor condensation on the wall in the vapor volume is calculated from the wall condensation equation derived from the mass and energy jump conditions on this interface (Todreas and Kazimi, 1990). The heat transfer coefficient for condensation is calculated using the model derived by Nusselt (shown in Holman, 1989). The wall temperature can be calculated solving a wall conduction equation with a heat transfer coefficient averaged over all volumes.

4. Heater simulation control

The pressurizer heaters are simulated using a time delay equation with a typical time constant. Therefore, the equation for the time behavior of the pressurizer heaters is (Baron, 1973)

$$\frac{d\dot{Q}_{\text{heater}}}{dt} = \frac{1}{\tau_h}\left(\dot{Q}_{\text{elect}}^{(t)} - \dot{Q}_{\text{heater}}\right) \tag{8a}$$

The proportional heater bank is controlled as (Barroso et al., 2003)

$$\dot{Q}_{\text{PI}}^{(t)} = \left[K_p\left(\frac{p_{\text{set}} - p}{p_{\text{set}}}\right) + K_i \int_{t_0}^{t} \left(\frac{p_{\text{set}} - p}{p_{\text{set}}}\right) dt\right] \dot{Q}_{\text{PI}}^{\text{Total}} + \dot{Q}_{\text{PI}}^{(t_0)} \tag{8b}$$

The proportional heater bank power is limited to the $\dot{Q}_{\text{PI}}^{\text{Total}}$ value. The back-up heater banks power is the design value when the pressure is within the interval of the prescribed pressure set points, and zero, when the pressure is outside this interval. The total electric power in the pressurizer electric heaters is the sum of the power of the proportional heater bank and the power of the back-up heater banks.

5. Model validation

This pressurizer model was compared to the experimental data of a 74 MW loss of load transient in the Shippingport reactor (Nahavandi and Makkenchery, 1970) using its heaters, spray, and relief valve specific controls. As shown in Fig. 1, the results for the three-volume and the two-volume models, using a separate solver, are almost identical. Both results show a very little discrepancy from results of the two-volume model using a simultaneous solver. Despite some uncertainty in the in-surge and spray enthalpy, the numeric results from these models are considered in good agreement with the Shippingport pressurizer experimental data.

6. IRIS pressurizer transient simulation

In IRIS, the pressurizer is located in the upper head of the integral vessel (for the reactor, steam generators, and main pumps), above the internal control rod mechanisms. This placement is considered optimal for the IRIS design, since it maximizes the overall pressurizer volume. The IRIS pressurizer layout is shown in the Fig. 2.

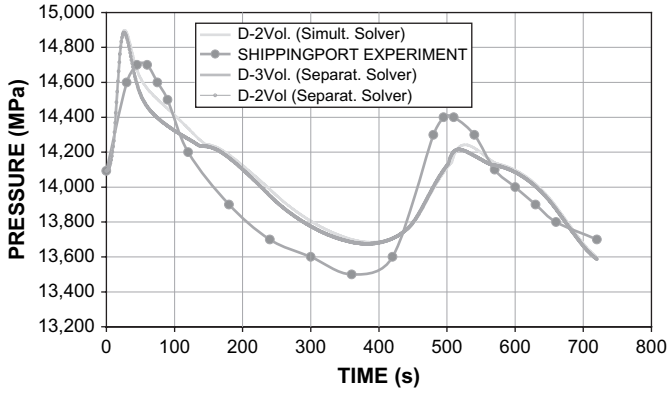

Fig. 1. Loss of load of the Shippingport reactor.

The three- and the two-volume models were used to simulate numerically a typical out-surge transient in the IRIS pressurizer. The driving parameter in this transient is the mass flow rate through the surge orifices, calculated in a primary circuit simulation (Barroso et al., 2003). The mass flow rate curve is shown in Fig. 3. In surge events, the pressure is controlled by the heater power. The heater power value calculated by the heater controller is shown in Fig. 4. Using the various numerical models, the pressure curves are shown in Fig. 5. Notice the pressure stabilization by the heater controller. The D-labeled results in Figs. 4 and 5 have the wall condensation energy terms explicitly represented in the energy equations. In the B-labeled results the wall condensation is contained in the heat transfer coefficient to calculate the heat losses to the pressurizer wall. As shown in Fig. 4, all results of the three-volume and the two-volume models are almost identical, using either a separate solver or a simultaneous solver. The B-labeled and the D-labeled software were developed independently, and a preliminary "validation" was performed for the D-labeled software.

The preliminary validation and the agreement of the curves demonstrate that the calculated pressure curves can correctly

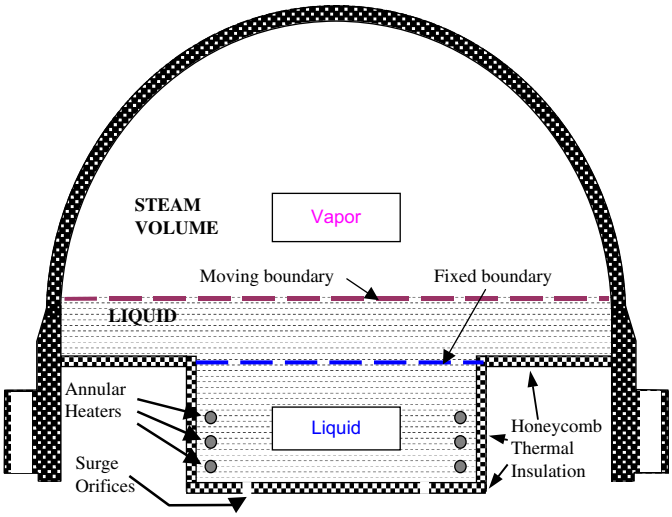

Fig. 2. The IRIS pressurizer layout.

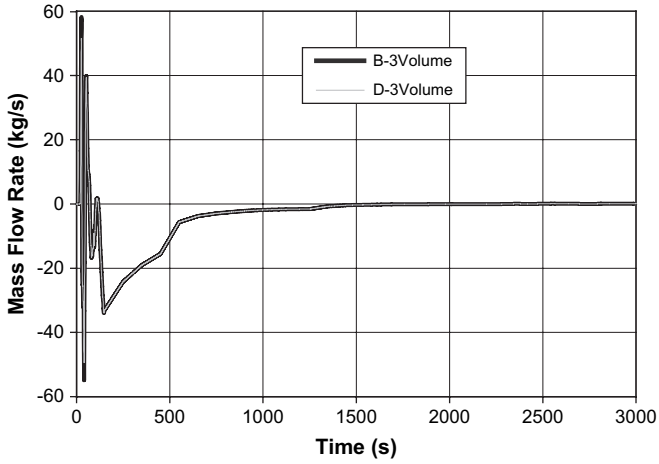

Fig. 3. Surge mass flow rate.

represent the response of the IRIS pressurizer to out-surge transients.

7. The non-dimensional mass and energy conservation equations

The non-dimensional mass and energy balance equations in the two-volume pressurizer are

$$\frac{\mathrm{d}}{\mathrm{d}t'}\left(m'_{\mathrm{v}}\right) = W'_{\mathrm{FL}} - W'_{\mathrm{RO}} - W'_{\mathrm{WC}} \tag{9}$$

$$\frac{\mathrm{d}}{\mathrm{d}t'}\left(m'_{\mathrm{l}}\right) = -W'_{\mathrm{FL}} + W'_{\mathrm{RO}} + W'_{\mathrm{WC}} + \dot{m}'_{\mathrm{surge}} \tag{10}$$

$$\frac{\mathrm{d}}{\mathrm{d}t'}\left(m'_{\mathrm{v}}h'_{\mathrm{v}}\right) = \left(W'_{\mathrm{FL}} - W'_{\mathrm{WC}}\right)h'_{\mathrm{g}} - W'_{\mathrm{RO}}\,h'_{\mathrm{f}} + \left(\frac{p^0 v^0_{\mathrm{fg}}}{h^0_{\mathrm{fg}}}\right)m'_{\mathrm{v}}v'_{\mathrm{v}}\frac{\mathrm{d}p'}{\mathrm{d}t'} \tag{11}$$

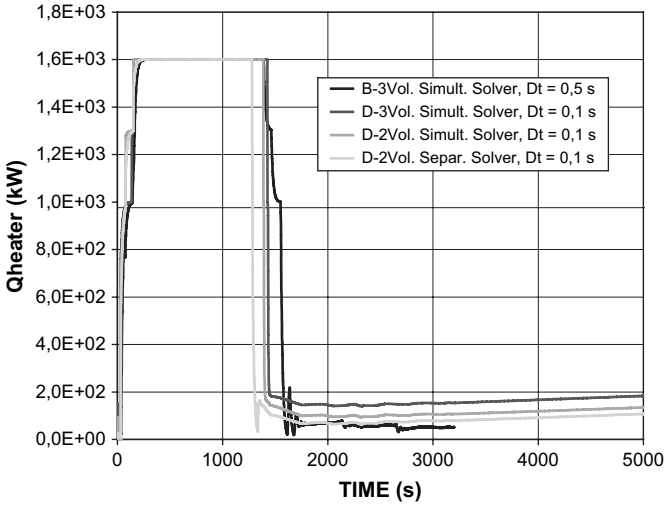

Fig. 4. The heater power control in the IRIS pressurizer.

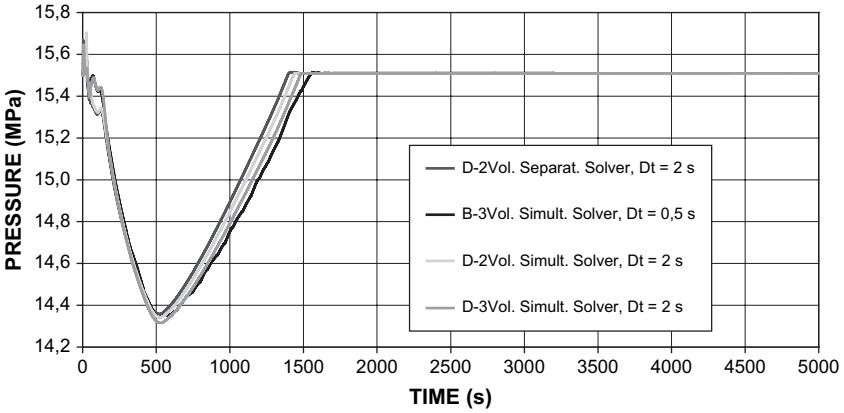

Fig. 5. The out-surge pressure transient in the IRIS pressurizer.

$$\frac{\mathrm{d}}{\mathrm{d}t'}\left(m_{\mathrm{l}}'h_{\mathrm{l}}'\right)=\left(W_{\mathrm{RO}}'+W_{\mathrm{WC}}'\right)h_{\mathrm{f}}'-W_{\mathrm{FL}}'h_{\mathrm{g}}'+\left(\frac{p^0v_{\mathrm{fg}}^0}{h_{\mathrm{fg}}^0}\right)m_{\mathrm{l}}'v_{\mathrm{l}}'\frac{\mathrm{d}p'}{\mathrm{d}t'}+\dot{m}_{\mathrm{surge}}'h_{\mathrm{surge}}'+\left(\frac{\dot{Q}_h^0}{\dot{m}_{\mathrm{surge}}^0h_{\mathrm{fg}}^0}\right)\dot{Q}_{\mathrm{heater}}' \tag{12}$$

The primed variables in Eqs. (9)–(12) are non-dimensional. The 0 superscript parameters are reference values. The m_{v}', m_{l}', h_{v}', and h_{l}' are the non-dimensional unknowns in these equations. The W_{FL}', W_{RO}', and W_{WC}' are non-dimensional mass flow rates which are obtained through specific non-dimensional constitutive equations. The constitutive equations, in turn, introduce new non-dimensional numbers, as defined later in this report. All other prime variables are non-dimensional that need to be made equal in a similar model. The similarity concept is defined later in this report. The surge mass flow rate prime variable is a given function that is equal in all scales. For in-surge, the surge enthalpy, h_{surge}', is a given function, that is the same in all scales. For out-surge, the surge enthalpy prime variable is a function of the solution, hence $h_{\mathrm{surge}}' = h_{\mathrm{l}}/h_{\mathrm{fg}}^0$.

The reference time used in Eqs. (9)–(12) is the reference mass divided by the reference mass flow rate. Due to this reference time, the mass equations introduce only the non-dimensional mass flow rates that, as mentioned, may introduce non-dimensional numbers through respective constitutive equations.

The prime variables, h_{f}' and h_{g}', in Eqs. (11) and (12) are expanded in the neighborhood of the reference pressure, respectively, as

$$h_{\mathrm{f}}'=\frac{h_{\mathrm{f}}}{h_{\mathrm{fg}}^0}=\frac{h_{\mathrm{f}}^0}{h_{\mathrm{fg}}^0}+\frac{p_0}{h_{\mathrm{fg}}^0}\left(\frac{\mathrm{d}h_{\mathrm{f}}}{\mathrm{d}p}\right)_0(p'-1) \tag{13}$$

$$h_{\mathrm{g}}'=\frac{h_{\mathrm{g}}}{h_{\mathrm{fg}}^0}=\frac{h_{\mathrm{g}}^0}{h_{\mathrm{fg}}^0}+\frac{p_0}{h_{\mathrm{fg}}^0}\left(\frac{\mathrm{d}h_{\mathrm{g}}}{\mathrm{d}p}\right)_0(p'-1) \tag{14}$$

Besides these non-dimensional, in the energy equations appear two additional non-dimensional factors: the pressure number and the heat source power number, which are, respectively, defined as

$$\left(NP_{\mathrm{pres}}^0\right)=\frac{p^0v_{\mathrm{fg}}^0}{h_{\mathrm{fg}}^0}=\Psi^0 \tag{15}$$

$$\left(N\dot{Q}_{\mathrm{heater}}^0\right)=\frac{\dot{Q}_h^0}{\dot{m}_{\mathrm{surge}}^0h_{\mathrm{fg}}^0} \tag{16}$$

8. The local phenomena

The closure equations in non-dimensional form represent the scaled mechanisms of rainout, flashing, and wall condensation. The model derived by Nusselt (Holman, 1989) defines the heat rate of wall condensation as

$$\dot{Q}_{\mathrm{WC}}=\frac{4k_{\mathrm{f}}}{3L_{\mathrm{v}}}\left(\frac{g\rho_{\mathrm{f}}(\rho_{\mathrm{f}}-\rho_{\mathrm{g}})h_{\mathrm{fg}}(L_{\mathrm{v}})^3}{4\mu_{\mathrm{f}}k_{\mathrm{f}}(T_{\mathrm{v}}-T_{\mathrm{w}})}\right)^{1/4}S_{\mathrm{v}}(T_{\mathrm{v}}-T_{\mathrm{w}}) \tag{17}$$

The non-dimensional form of Eq. (17) is

$$\dot{Q}_{\mathrm{WC}}'=\left(N\dot{Q}_{\mathrm{WC}}^0\right)h_{\mathrm{WC}}'S_{\mathrm{v}}'\left(T_{\mathrm{v}}'-T_{\mathrm{w}}'\right) \tag{18}$$

where the wall condensation heat number is defined as

$$\left(N\dot{Q}_{\mathrm{WC}}^0\right)=\frac{4}{3}\left(\frac{g(\rho^0)^2h^0(L^0)^3}{4\mu^0k^0T^0}\right)^{1/4}\left(\frac{A^0k^0T^0/L^0}{\dot{Q}_h^0}\right) \tag{19}$$

The mass flow rate associated to wall condensation is

$$W_{\mathrm{WC}}=\frac{\dot{Q}_{\mathrm{WC}}}{h_{\mathrm{fg}}} \tag{20}$$

The non-dimensional form of the wall condensation Eq. (20) is

$$W_{\mathrm{WC}}'=\frac{\dot{Q}_h^0\dot{Q}_{\mathrm{WC}}'}{\dot{m}_{\mathrm{surge}}^0h_{\mathrm{fg}}^0h_{\mathrm{fg}}'}=\left(N\dot{Q}_{\mathrm{heater}}^0\right)\left(N\dot{Q}_{\mathrm{WC}}^0\right)\frac{h_{\mathrm{WC}}'s_{\mathrm{v}}'\left(T_{\mathrm{v}}'-T_{\mathrm{w}}'\right)}{h_{\mathrm{fg}}'} \tag{21}$$

Eq. (13) defines a mass flow wall condensation number as

Table 1
Distortion in the pressure number with reduced pressure

Pressure P (MPa)	$P \times V_f/H_{fg}$	$\Psi m = P \times V_{fg}/H_{fg}$	$\varepsilon = (1 - \Psi m/\Psi p)$
15.5	2.737E−02	$\Psi p = 0.13038$	0.0000E+00
10.0	1.102E−02	1.2581E−01	3.1490E−02
5.0	3.928E−03	1.1636E−01	1.0470E−01
2.5	1.6280E−03	1.0699E−01	1.7940E−01
0.5	2.5900E−04	8.8600E−02	3.1790E−01
0.2	9.6000E−05	8.0300E−02	3.8180E−01

$$\left(NW^0_{WC}\right) = \left(N\dot{Q}^0_{heater}\right)\left(N\dot{Q}^0_{WC}\right) \tag{22}$$

Liquid drops are generated in the vapor volume due to bulk condensation (rainout) and flow through the liquid interface. The drag force is neglected because the acceleration resulting from the drop weight and the buoyancy reaction force is small in the equation of motion of a single liquid drop. The non-dimensional equation of motion of a liquid drop is

$$\frac{d^2y'}{dt'^2} = \left(\frac{gL_0}{u_0^2}\right)\left(\frac{\rho'_f - \rho'_g}{\rho'_f}\right) \tag{23}$$

The similarity number for the local phenomena of rainout is defined as the inverse of the Froude number. The rainout number and the Froude number are defined as

$$\left(NW^0_{RO}\right) = \frac{1}{Fr} = \frac{gL^0}{u_0^2} \tag{24}$$

The rainout mass flow rate is

$$W_{RO} = \rho_f u_d (1 - \alpha_v) A_{lv} \tag{25}$$

where the velocity that the liquid drop reaches the liquid interface is

$$u_d = \sqrt{gL_v\left(\frac{v_v - v_f}{v_v}\right)} \tag{26}$$

The non-dimensional form of the rainout mass flow rate Eq. (25) is

$$W'_{RO} = \frac{\rho'_f \rho^0 u'_d u^0 (1 - \alpha_v) A^0 A'_{lv}}{\dot{m}^0_{surge}} = (1 - \alpha_v)\rho'_f u'_d A'_{lv} \tag{27}$$

Vapor bubbles are generated in the liquid volume due to bulk evaporation (flashing) and flow through the liquid interface into the vapor volume. Because the acceleration resulting from the bubble weight and the buoyancy reaction force is large, it is necessary to include the drag force in the equation of motion of a vapor bubble in the liquid volume. If the bubble terminal velocity is calculated using the Zuber formula (Whalley, 1996),

$$u_b = 1.41\left[\frac{\sigma g(\rho_f - \rho_g)}{\rho_f^2}\right]^{1/4} \tag{28}$$

the non-dimensional equation of motion of a vapor bubble is

$$\frac{d^2y'}{dt'^2} = \left(\frac{\Delta\rho}{\rho_g}\right)^0 \frac{gL_0}{u_0^2}\left(\frac{\rho'_f - \rho'_g}{\rho'_g}\right) - \left[\left(\frac{\Delta\rho}{\rho_g}\right)^0 \frac{g\rho^0 (L^0)^2}{\sigma^0}\right]^{1/2} \frac{1}{2}\left[\frac{\rho'_f - \rho'_g}{\rho'_g}\left(\frac{\rho'_f}{\rho'_g}\right)\frac{\rho'_f}{\sigma'}\right]^{1/2}\left(\frac{dy'}{dt'}\right)^2 \tag{29}$$

The reference difference density ratio is fixed for a given pressure. The Froude number, Fr, equivalence is necessary for the rainout similarity. The flashing number is obtained from the ratio of square of the non-dimensional factor that appears in the drag force, to the non-dimensional factor in the gravitational force term of Eq. (29). The flashing number is thus defined as

$$\left(NW^0_{FL}\right) = \left(\frac{\Delta\rho}{\rho_g}\right)^0 \rho_f^0 \frac{L^0 u_0^2}{\sigma^0} \tag{30}$$

If the bubble terminal velocity is calculated using the Wilson formula (Wilson et al., 1961),

$$u_b = \gamma_1\left[g\left(\frac{\sigma}{g(\rho_f - \rho_g)}\right)^{0.5}\right]^{0.5} \tag{31}$$

the non-dimensional equation of motion of a vapor bubble is

$$\frac{d^2y'}{dt'^2} = \left(\frac{\Delta\rho}{\rho_g}\right)^0 \frac{gL_0}{u_0^2}\left(\frac{\rho'_f - \rho'_g}{\rho'_g}\right) - \frac{1}{\gamma_1^2}\left(\frac{\Delta\rho}{\rho_g}\right)^0 \left(\frac{\rho'_f - \rho'_g}{\rho'_g}\right) \times \left(\rho_f^0 \frac{gL_0^2}{\sigma^0}\right)^{0.5}\left(\frac{\rho'_f - \rho'_g}{\sigma'}\right)^{0.5}\left(\frac{dy'}{dt'}\right)^2 \tag{32}$$

The bubble non-dimensional velocity, γ_1, is assumed, in the model pressurizer, of the same magnitude of that in the IRIS pressurizer. Therefore, the same Eq. (22), expression, for the

Table 2
Ranges of the pressurizer variables

Hemispheric radius (m)	Surge mass flow rate (kg)	Heating power (kW)
0.31115−3.11150	5.484−54.840	10.0−1000.0

Table 3
Consistency test data for the IRIS pressurizer

Pressure (MPa)	Hemispheric radius (m)	Surge mass flow rate (maximum) (kg/s)	Heating power (maximum) (kW)
15.5	3.1115	54.84	1000.00
15.5 (*)	3.0239	51.75	937.61

Table 4
PI controller numbers for the IRIS pressurizer

Pressure (MPa)	NK^0_p	NK^0_i
15.5	3.4392E+00	9.7672E−09
15.5 (*)	3.4392E+00	9.7672E−09

Table 5
Size data for the model pressurizer

Pressure (MPa)	Hemispheric radius (m)	Surge mass flow rate (maximum) (kg/s)	Heating power (maximum) (kW)
15.5	3.1115E+00	5.4840E+01	1.0000E+03
10.0	2.6434E+00	5.1172E+01	5.5844E+02
5.0	1.6512E+00	3.0000E+01	1.5000E+02
2.5	1.2394E+00	2.0000E+01	6.0000E+01
0.5	1.5237E+00	2.5000E+01	2.5000E+01
0.2	1.5285E+00	1.0000E+01	6.1877E+00

flashing number is obtained. In the second derivation, the flashing number is also defined as the ratio of square of the non-dimensional factor that appears in the drag force, to the non-dimensional factor in the gravitational force term of Eq. (32).

The flashing mass flow rate is

$$W_{\mathrm{FL}} = \rho_{\mathrm{g}} u_{\mathrm{b}} \alpha_{\mathrm{l}} A_{\mathrm{lv}} \tag{33}$$

The non-dimensional form of the flashing mass flow rate Eq. (33) is

$$W'_{\mathrm{FL}} = \frac{\rho'_{\mathrm{g}} \rho^0 u'_{\mathrm{b}} u^0 \alpha_{\mathrm{l}} A^0 A'_{\mathrm{lv}}}{\dot{m}^0_{\mathrm{surge}}} = \alpha_{\mathrm{l}} \rho'_{\mathrm{g}} u'_{\mathrm{b}} A'_{\mathrm{lv}} \tag{34}$$

The substitution of Eqs. (13) and (14) into the Eqs. (11) and (12) introduce eight new non-dimensional numbers. As the rainout mass flow Eq. (27) and the flashing mass flow Eq. (34) do not introduce new non-dimensional numbers, the similarity numbers associated with the enthalpy transport by rainout and flashing are defined, respectively, as

$$\left(NWh^0_{\mathrm{RO}}\right)_1 = \frac{h^0_{\mathrm{f}}}{h^0_{\mathrm{fg}}} \tag{35}$$

$$\left(NWh^0_{\mathrm{RO}}\right)_2 = \frac{p_0}{h^0_{\mathrm{fg}}}\left(\frac{\mathrm{d}h_{\mathrm{f}}}{\mathrm{d}p}\right)_0 \tag{36}$$

$$\left(NWh^0_{\mathrm{FL}}\right)_1 = \frac{h^0_{\mathrm{g}}}{h^0_{\mathrm{fg}}} \tag{37}$$

$$\left(NWh^0_{\mathrm{FL}}\right)_2 = \frac{p_0}{h^0_{\mathrm{fg}}}\left(\frac{\mathrm{d}h_{\mathrm{g}}}{\mathrm{d}p}\right)_0 \tag{38}$$

As the mass flow wall condensation Eq. (21) introduces the mass flow wall condensation number, defined in Eq. (22), the similarity numbers associated with the enthalpy transport by wall condensation are defined as

$$\left(NWh^0_{\mathrm{WC}}\right)_1 = \left(NW^0_{\mathrm{WC}}\right)\frac{h^0_{\mathrm{f}}}{h^0_{\mathrm{fg}}} \tag{39}$$

$$\left(NWh^0_{\mathrm{WC}}\right)_2 = \left(NW^0_{\mathrm{WC}}\right)\frac{h^0_{\mathrm{g}}}{h^0_{\mathrm{fg}}} \tag{40}$$

$$\left(NWh^0_{\mathrm{WC}}\right)_3 = \left(NW^0_{\mathrm{WC}}\right)\frac{p_0}{h^0_{\mathrm{fg}}}\left(\frac{\mathrm{d}h_{\mathrm{f}}}{\mathrm{d}p}\right)_0 \tag{41}$$

$$\left(NWh^0_{\mathrm{WC}}\right)_4 = \left(NW^0_{\mathrm{WC}}\right)\frac{p_0}{h^0_{\mathrm{fg}}}\left(\frac{\mathrm{d}h_{\mathrm{g}}}{\mathrm{d}p}\right)_0 \tag{42}$$

Table 7
Similarity numbers for the IRIS and the model pressurizer (B)

Pressure (MPa)	$(NW^0_{\mathrm{RO}})_1$	$(NW^0_{\mathrm{RO}})_2$	$(NW^0_{\mathrm{FL}})_1$	$(NW^0_{\mathrm{FL}})_2$
15.5	1.687E+00	6.349E−01	2.687E+00	4.744E−01
15.5 (*)	1.687E+00	6.349E−01	2.687E+00	4.744E−01
10.0	1.069E+00	3.268E−01	2.069E+00	1.372E−01
5.0	7.041E−01	1.899E−01	1.704E+00	2.490E−02
2.5	5.228E−01	1.335E−01	1.523E+00	6.555E−03
0.5	3.037E−01	7.668E−02	1.304E+00	2.138E−02
0.2	2.292E−01	6.056E−02	1.230E+00	2.194E−02

9. The PI controler

In a transient of out-surge, the pressure can be controlled by a PI controller (Barroso et al., 2003). The equation for the heater bank control can be put in a non-dimensional form as

$$\dot{Q}'_{\mathrm{heater}} = \dot{Q}'_{\mathrm{PI}} = K_{\mathrm{p}}(1-p') + \frac{m^0 K_{\mathrm{i}}}{\dot{m}^0}\int_{t'_0}^{t'}(1-p')\mathrm{d}t' \tag{43}$$

As the PI controller is employed to simulate the dynamic behavior of the pressurizer, the substitution of Eq. (43) into Eq. (12) defines new similarity numbers. These new similarity numbers are the proportional and integral numbers, defined respectively, as

$$\left(NK^0_{\mathrm{p}}\right) = K_{\mathrm{p}}\left(\frac{\dot{Q}^0_h}{\dot{m}^0_{\mathrm{surge}} h^0_{\mathrm{fg}}}\right) \tag{44}$$

Table 6
Similarity numbers for the IRIS and the model pressurizer (A)

Pressure (MPa)	$(NW^0_{\mathrm{WC}})_0$	$(NW^0_{\mathrm{WC}})_1$	$(NW^0_{\mathrm{WC}})_2$	$(NW^0_{\mathrm{WC}})_3$	$(NW^0_{\mathrm{WC}})_4$
15.5	3.281E−01	5.534E−01	2.083E−01	8.815E−01	1.556E−01
15.5 (*)	3.329E−01	5.614E−01	2.113E−01	8.943E−01	1.579E−01
10.0	5.101E−01	5.450E−01	1.667E−01	1.106E+00	6.995E−02
5.0	8.708E−01	6.131E−01	1.654E−01	1.484E+00	2.169E−02
2.5	1.255E+00	6.562E−01	1.675E−01	1.911E+00	8.228E−04
0.5	3.296E+00	1.001E+00	2.527E−01	4.297E+00	7.047E−02
0.2	1.082E+01	2.481E+00	6.554E−01	1.330E+01	2.277E−01

Table 8
Similarity numbers for the IRIS and the model pressurizer

Pressure (MPa)	(NP^0_{pres})	$N\dot{Q}^0_{WC}$	NW^0_{RO}	NW^0_{FL}	FIT
15.5	1.304E−01	1.739E+01	8.557E+05	3.581E+01	
15.5 (*)	1.304E−01	1.764E+01	8.330E+05	3.474E+01	1.381E−02
10.0	1.258E−01	2.703E+01	5.834E+05	4.092E+01	3.695E−01
5.0	1.164E−01	4.615E+01	2.059E+05	6.835E+01	8.169E−01
2.5	1.070E−01	6.652E+01	1.274E+05	1.047E+02	1.292E+00
0.5	8.860E−02	1.747E+02	2.749E+05	2.787E+02	3.906E+00
0.2	8.030E−02	5.735E+02	1.853E+06	9.216E+01	1.230E+01

$$\left(NK^0_{\mathrm{i}}\right) = \frac{m^0 K_{\mathrm{i}}}{\dot{m}^0_{\mathrm{surge}}}\left(\frac{\dot{Q}^0_h}{\dot{m}^0_{\mathrm{surge}} h^0_{\mathrm{fg}}}\right) \tag{45}$$

These PI controller numbers of Eqs. (44) and (45) substitute the heat source number.

10. Similarity

In general, similar systems are those represented by the same equations. For similarity, it is sufficient the equality of all the corresponding similarity numbers of the scaled models and the full-scale system. In a scale optimization, the values of the similarity numbers are used to define the parameters of the scaled system. Due to the impossibility to match the prime variables (that are not the unknowns) with different pressure, it can be attained only an approximate similarity. The pressure numbers of the full scale and of the scaled systems with smaller pressure are shown in the third column of Table 1.

All scaled models with smaller pressure can only be designed with approximate similarity, due to the distortion in the pressure number. The pressure number as defined in Table 1 has ''self similarity'', which is defined as the repetition of details at descending scales (Reyes and Hochreiter, 1998). If the liquid density were defined as reference (column 2), the resulting pressure number would be much more distorted. The last column of Table 1 shows the distortion in the pressure number with reduced pressure.

11. Genetic algorithm optimization

Genetic algorithms (GAs) (Goldberg, 1989) are optimization methods inspired in the evolution theory, in which artificial chromosomes composed of binary numbers (genes) encode solution candidates. In this work, the chromosome encodes the list of search variable. In the GA, initially a population of chromosomes is randomly generated. Then, guided by a fitness function (the objective function of the optimization problem), the evolution takes place by simulated natural selection, crossovers and mutations. By such operations, the solution candidates (chromosomes) are improved from generation to generation. One of the first applications of GA to design a thermal–hydraulic experiment can be seen in Lapa et al. (2004).

In this work, the pressure of a scaled experiment is fixed, but exist complex dependencies of the similarity numbers on the size and operation parameters. The search variables are the radius of the hemisphere of the pressurizer, the surge mass flow rate, and the heater thermal power. Eq. (46) defines the fitness function as the overall difference between all corresponding similarity numbers of the scaled experiment and the original pressurizer. The similarity numbers with superscript, ''P'', are for the full-scale pressurizer, and those with superscript, ''m'', are of the scaled experiment.

Fixing the pressure of a scaled model, one search variable is the radius of the hemisphere as in the IRIS pressurizer (Barroso and Batista Fo, 2004). The other dimensions are in a linear proportion. The remaining search variables are the

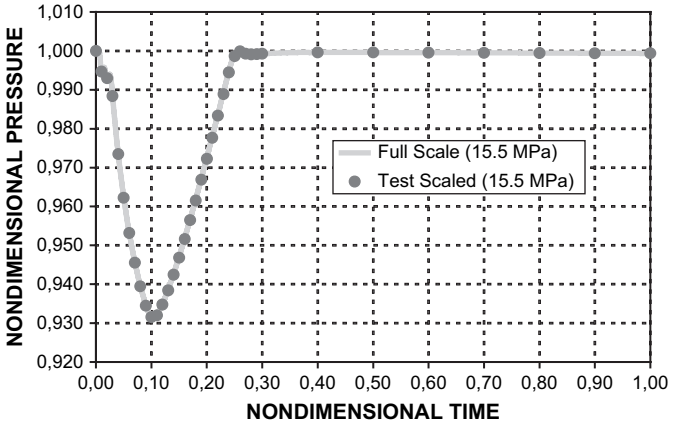

Fig. 6. Non-dimensional pressure for the similar pressurizer with same pressure.

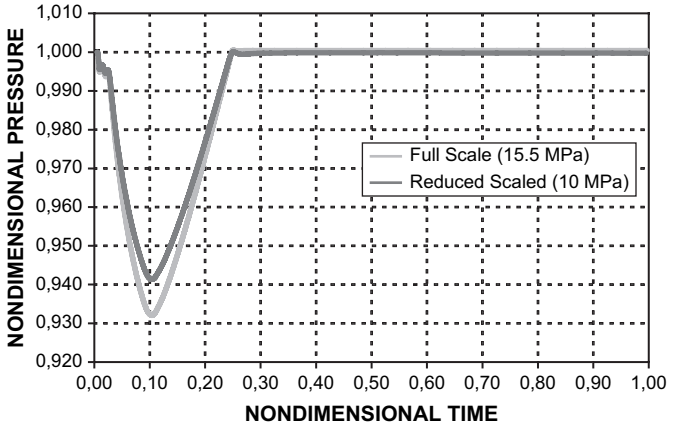

Fig. 7. Non-dimensional pressure for IRIS and the model pressurizer (10 MPa).

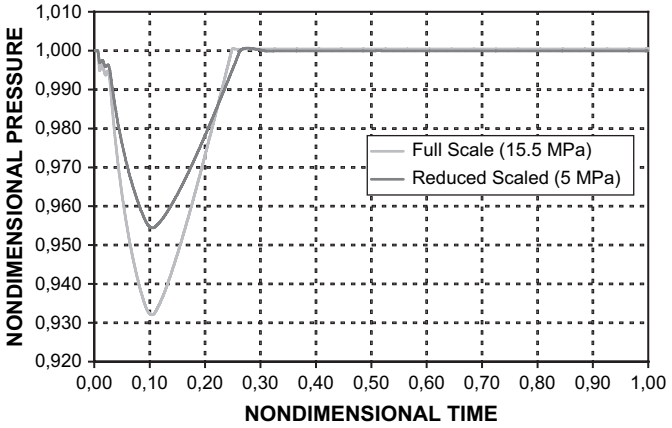

Fig. 8. Non-dimensional pressure for IRIS and the model pressurizer (5 MPa).

surge mass flow rate and the heater thermal power. Several sets of these variables are defined and tested by the genetic algorithm (GA).

$$\mathrm{FIT} = \sqrt{\frac{\sum_{i=0}^{14} w_i \left(1 - N_{\mathrm{i}}^{\mathrm{m}}/N_{\mathrm{i}}^{\mathrm{P}}\right)^2}{\sum_{i=0}^{14} w_i}} \tag{46}$$

In Eq. (46) $N_{\mathrm{i}}^{\mathrm{P}}$ represent the similarity numbers of the IRIS pressurizer and $N_{\mathrm{i}}^{\mathrm{m}}$ those of the scaled model, as defined in the Nomenclature, and w_i are weighting numbers. The weighting numbers used were $w_0 = w_1 = \cdots = w_{14} = 1$.

The out-surge test transient in IRIS pressurizer is driven by a mass flow rate curve having a maximum (negative) of −54.84 kg/s (Barroso and Batista Fo, 2004). An adequate PI controller can control the transient. The maximum heat power of the proportional bank of the PI controller is 1 MW. This transient requires different sizes for scaled models, as defined by GA. The parameters of the PI controller can also be calculated by GA, and was done for the consistency test. Nevertheless, it was observed that the GA search always matched the similarity numbers of the controller. Therefore, the parameters of the controller of the models with reduced pressure were calculated from the exact equality of their corresponding similarity numbers.

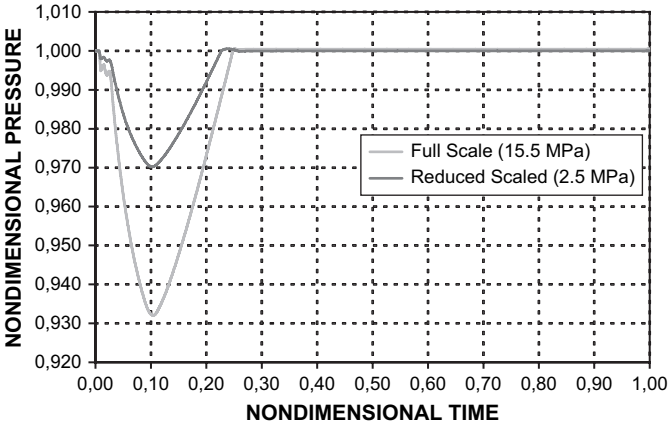

Fig. 9. Non-dimensional pressure for IRIS and the model pressurizer (2.5 MPa).

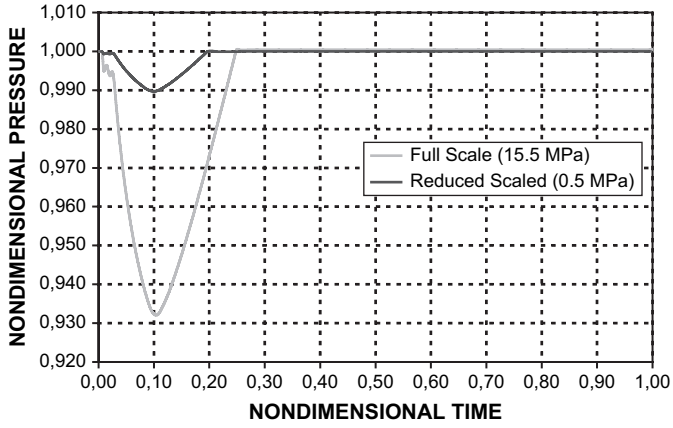

Fig. 10. Non-dimensional pressure for IRIS and the model pressurizer (0.5 MPa).

The consistency of the method is verified searching the parameters of a full pressure system similar to the IRIS pressurizer. In the GA search, the ranges of the search variables are shown in Table 2. The obtained variables are shown in Table 3.

The consistency test in the PI controller numbers of the scaled system of Table 3 is shown in Table 4. The size data of the small-scaled models are shown in Table 5. The similarity numbers for the models are shown in Tables 6–8. An asterisk marks the consistency data in these tables. It is shown that the similar pressurizer in the same pressure reaches excellent agreement in all similarity numbers for a final discrepancy of ∼0.0138 in the final fitness function. Fig. 6 shows the good agreement also obtained for the non-dimensional pressure curve of the out-surge transient for the similar pressurizer with same pressure.

The similarity numbers of the controller of all models match the respective numbers of IRIS pressurizer, presented in Table 4. As expected, the discrepancy in the similarity numbers increases when the pressure decreases. It is shown by the relative deviation in the wall condensation number, that the local phenomena most difficult to attain similarity in a much-reduced pressure are wall condensation. The deviations in the similarity numbers cause the distortion in the solution of the pressurizer Eqs. (9)–(12) for the small-scaled models.

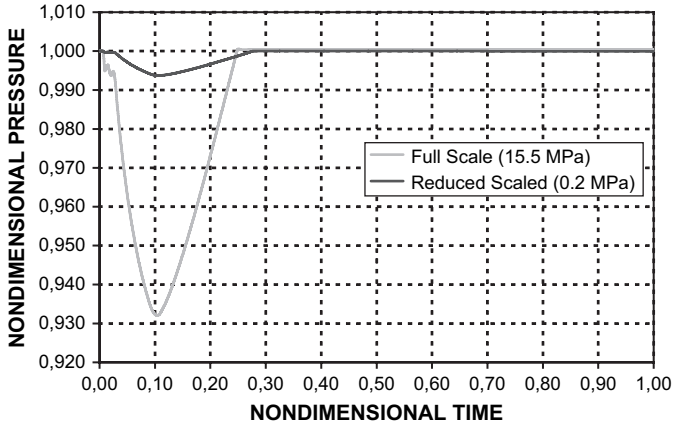

Fig. 11. Non-dimensional pressure for IRIS and the model pressurizer (0.2 MPa).

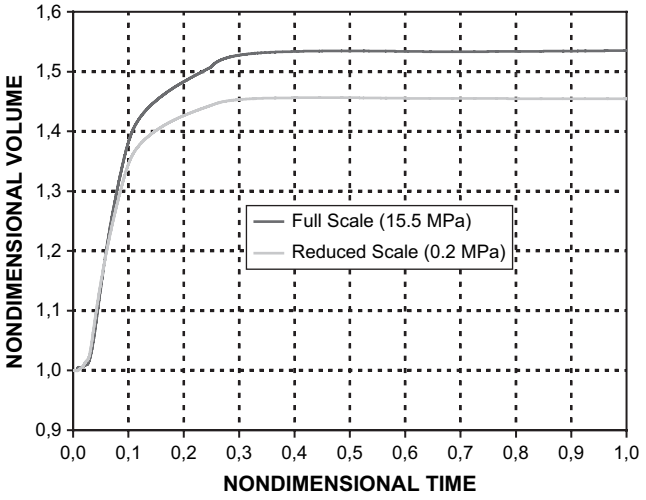

Fig. 12. The vapor volume for the IRIS and the model pressurizer.

Figs. 7–11 show the degree of agreement that can be obtained for the non-dimensional pressure curve of the outsurge transient of the similar pressurizer with reduced pressures. Despite the fact that experiments with much-reduced pressure as 0.2 MPa or 0.5 MPa, have much distorted non-dimensional pressure, the variation in the pressure still permit experimental measurement for code validation. A much better experiment, the 2.5 MPa experiment, certainly is adequate and acceptable by the licensing authority for code validation.

Despite the discrepancy in these numbers, the transient simulations, presented in Figs. 7–11, show that the non-dimensional pressure curves of the models tend to the curve of the IRIS pressurizer prototype when the pressure of the models increases. It is observed that the non-dimensional time for the minimum pressure is approximately the same in all scaled models.

Although the largest distorted pressure is for the model with 0.2 MPa, the non-dimensional vapor and liquid volumes still show good agreement with the IRIS transient results, as shown, respectively, in Figs. 12 and 13.

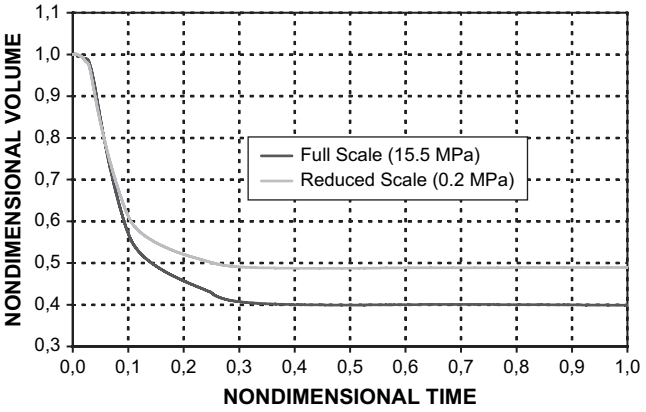

Fig. 13. The liquid volume for the IRIS and the model pressurizer.

12. Conclusions

As shown, the results of the three-volume and the two-volume models are almost identical, using either a separate solver or a simultaneous solver. The preliminary validation, using the Shippingport experimental data, and the close agreement reached by all the developed software, for the IRIS outsurge transient, recommends further validation of these models for the test evaluation and the design of scaled experiments for the IRIS pressurizer.

Because of the smaller distortion in the pressure number, the form obtained of the non-dimensional mass and energy equations shall always be used. The derivation of non-dimensional constitutive models is of great relevance to scale the local phenomena of rainout, flashing and wall condensation in a scaled model. The GA defined the model parameters (size, flow rate, power, and the PI control constants). For this definition, the sum of the square of the differences between respective similarity numbers was minimized. This GA optimization is a much valuable tool to obtain the parameters for the model. Without the GA or other good optimization algorithm, the individual designer would have much difficulty to define the best parameters. The agreement of the non-dimensional pressure as the model pressure increases, and the good agreement of the non-dimensional volumes of different scaled systems recommend this non-dimensional formalism, the GA optimization, and the numeric simulation of a surge transient, to design scaled experiments for modeling the IRIS pressurizer.

References

Barroso, A.C.O., Batista Fo., B.D., 2004. Refining the design of the IRIS pressurizer. In: Proceeding of the 5th International Conference on Nuclear Option in Countries with Small and Medium Electricity Grids, Dubrovnik, Croatia.

Barroso, A.C.O., Batista Fo., B.D., Arone, I.D., Macedo, L.A., de Sampaio, P.A.B., Morais, M., 2003. IRIS pressurizer design. In: Proceedings of the ICAPP, Cordoba, Spain, Paper 3227.

Baron, R.C., 1973. Digital model simulation of a nuclear pressurizer. Nuclear Science and Engineering 52, 283–291.

Goldberg, D.E., 1989. Genetic Algorithms in Search, Optimization and Machine Learning. Addison-Wesley.

Holman, J.P., 1989. Heat Transfer. McGraw-Hill Book Company, Singapore.

Kang, S.-W., Griffith, P., 1984. Pool heat transfer in a simulated PWR pressurizer. Transactions of the American Nuclear Society 46, 845–847.

Lapa, C.M.F., de Sampaio, P.A.B., Pereira, C.M.N.A., 2004. A new approach to designing reduced scale thermal–hydraulic experiments. Nuclear Engineering and Design 229 (2–3), 205–212.

Nahavandi, A.N., Makkenchery, S., 1970. An improved pressurizer model with bubble rise and condensate drop dynamics. Nuclear Engineering and Design 12, 135–147.

Reyes Jr., J.N., Hochreiter, L., 1998. Scaling analysis of the OSU AP600 test facility (APEX). Nuclear Engineering and Design 186, 53–109.

Todreas, N.E., Kazimi, M.S., 1990. Nuclear Systems I, Thermal Hydraulic Fundamentals. Taylor & Francis, Levittown, USA.

Wilson, J.F., Grenda, R.J., Patterson, J.F., 1961. Steam volume fraction in a bubbling two-phase mixture. Transactions of the American Nuclear Society 4 (section 37), 356–357.

Whalley, P.B., 1996. Two-Phase Flow and Heat Transfer. Oxford University Press, New York.